PHYSICAL REVIEW C **92**, 041303(R) (2015)

Investigation into the semimagic nature of the tin isotopes through electromagnetic moments

J. M. Allmond,[1] A. E. Stuchbery,[2] A. Galindo-Uribarri,[1,3] E. Padilla-Rodal,[4] D. C. Radford,[1] J. C. Batchelder,[5] C. R. Bingham,[1,3] M. E. Howard,[6] J. F. Liang,[1] B. Manning,[6] S. D. Pain,[1] N. J. Stone,[3,7] R. L. Varner,[1] and C.-H. Yu[1]

[1]*Physics Division, Oak Ridge National Laboratory, Oak Ridge, Tennessee 37831, USA*
[2]*Department of Nuclear Physics, Australian National University, Canberra ACT 2601, Australia*
[3]*Department of Physics and Astronomy, University of Tennessee, Knoxville, Tennessee 37996, USA*
[4]*Instituto de Ciencias Nucleares, UNAM, AP 70-543, 04510 Mexico, D.F., Mexico*
[5]*UNIRIB, Oak Ridge Associated Universities, Oak Ridge, Tennessee 37831, USA*
[6]*Department of Physics and Astronomy, Rutgers University, New Brunswick, New Jersey 08903, USA*
[7]*Department of Physics, Oxford University, Oxford, OX1 3PU, United Kingdom*

(Received 22 July 2015; revised manuscript received 30 September 2015; published 19 October 2015)

A complete set of electromagnetic moments, $B(E2;0_1^+ \rightarrow 2_1^+)$, $Q(2_1^+)$, and $g(2_1^+)$, have been measured from Coulomb excitation of semimagic ^{112,114,116,118,120,122,124}Sn ($Z = 50$) on natural carbon and titanium targets. The magnitude of the $B(E2)$ values, measured to a precision of ∼4%, disagree with a recent lifetime study [Phys. Lett. B **695**, 110 (2011)] that employed the Doppler-shift attenuation method. The $B(E2)$ values show an overall enhancement compared with recent theoretical calculations and a clear asymmetry about midshell, contrary to naive expectations. A new static electric quadrupole moment, $Q(2_1^+)$, has been measured for ^{114}Sn. The static quadrupole moments are generally consistent with zero but reveal an enhancement near midshell; this had not been previously observed. The magnetic dipole moments are consistent with previous measurements and show a near monotonic decrease in value with neutron number. The g-factor measurements in ^{112,114}Sn establish the recoil-in-vacuum method for states with $\tau \sim 0.5$ ps and hence demonstrate that this method can be used for future g-factor measurements on proton-rich isotopes toward ^{100}Sn. Current theory calculations fail to reproduce the electromagnetic moments of the tin isotopes. The role of 2p-2h and 4p-4h intruders, which are lowest in energy at midshell and outside of current model spaces, needs to be investigated in the future.

DOI: 10.1103/PhysRevC.92.041303 PACS number(s): 25.70.De, 21.10.Ky, 23.20.−g, 27.60.+j

The tin isotopes, which have a closed proton shell of $Z = 50$, constitute the longest chain of semimagic nuclei with 15 even-even isotopes between the ^{100}Sn ($N = 50$) and ^{132}Sn ($N = 82$) double-shell closures. Seven of these isotopes are stable and eight are unstable. These features have made the tin isotopes a prototypical benchmark of state-of-the-art microscopic theory and experiment and a rich arena for investigating residual nucleon-nucleon interactions. With the advent of radioactive ion beams and access to both neutron-rich and proton-rich isotopes, interest in the tin isotopes has been compounded. This interest is reflected in the large number of both experimental [1–18] and theoretical [19–29] studies of the first 2^+ states of the even-even tin isotopes in the past decade.

While radioactive ^{132}Sn is a robust double-shell closure [1,10,17,30–33], electric quadrupole transition probabilities $B(E2;0_1^+ \rightarrow 2_1^+)$ for the proton-rich tin isotopes have shown enhanced 2_1^+ collectivity when moving towards ^{100}Sn [2–4,6,12,13], suggesting that the ^{100}Sn core is soft to excitations. On the other hand, a recent systematic lifetime study of the stable even-even tin isotopes by Jungclaus *et al.* [9] observed a dramatic departure from the $B(E2)$ values of the Raman evaluation [34], with a decrease in collectivity near midshell. The local minimum at midshell, which coincides with a possible $N = 64$ subshell closure, was interpreted as a reduction in collectivity due to the influence of the $s_{1/2}$ orbital, which cannot form a 2^+ state from the coupling of two neutrons. The interpretation was supported by a subsequent generalized seniority calculation [23]. The recent $B(E2)$ discrepancies between the study of Jungclaus *et al.* [9] and the Raman evaluation [34] have remained an outstanding experimental problem since 2011 and have complicated the interpretation [10–13,23,24,26–28] of both the stable and exotic tin isotopes. There has been theoretical work directed toward reproducing the new lifetime results of Jungclaus *et al.* [23,26,28], and there have been Coulomb-excitation studies of proton-rich tin isotopes [2,11] measured relative to ^{112}Sn; the $B(E2)$ values from these studies would be 17% smaller if normalized to the results of Jungclaus *et al.*, weakening the evidence for enhanced collectivity toward ^{100}Sn.

In this Rapid Communication, we report a complete set of electromagnetic moments, $B(E2;0_1^+ \rightarrow 2_1^+)$, $Q(2_1^+)$, and $g(2_1^+)$, from Coulomb excitation of semimagic ^{112,114,116,118,120,122,124}Sn on natural carbon and titanium targets with an experimental setup that has been optimized for absolute $B(E2)$ measurements for over a decade [35]. The magnitude of the present $B(E2)$ values disagree with the recent Doppler-shift attenuation lifetime study by Jungclaus *et al.* [9] but there is a clear asymmetry about midshell with a possible local minimum at midshell. The increase in collectivity reported for the proton-rich nuclei is observed already for the two lightest stable tin isotopes. A new trend is observed in the static electric quadrupole moments, $Q(2_1^+)$, which resembles a bell shape with a maximum at midshell. The magnetic dipole moments, $g(2_1^+)$, show a near-monotonic decrease in value with neutron number. The complete set of electromagnetic moments in the present systematic study permits a unique investigation into the semimagic nature of the

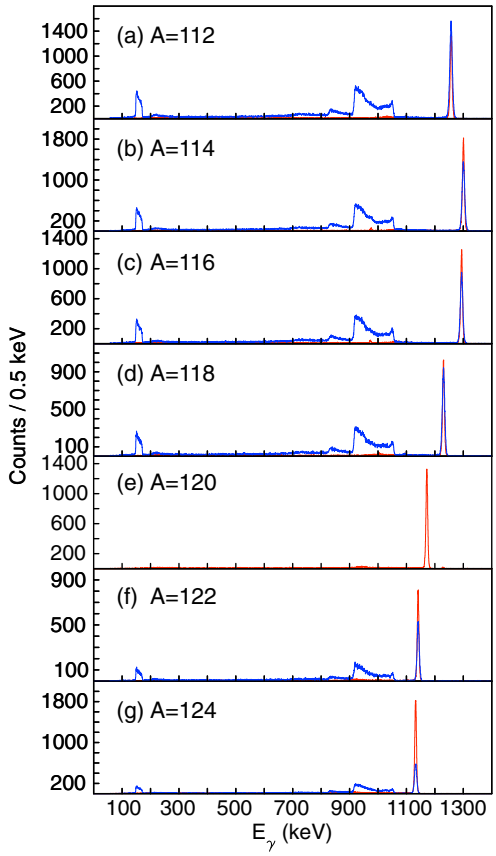

FIG. 1. (Color online) Panels (a)–(g) show the $2_1^+ \rightarrow 0_1^+$ γ-ray transitions of $^{112-124}$Sn, respectively, from Coulomb excitation on carbon (red) and titanium (blue) targets. ^{120}Sn on titanium was omitted due to beam-time constraints.

tin isotopes; all three observables show a change in behavior around midshell.

Ion beams of ^{112,114,116,118,120,122,124}Sn at an energy of 2.9 MeV per nucleon were Coulomb excited on 1.01 and 1.09 mg/cm^2 natural carbon and titanium targets, respectively, over a period of ten days. The beams were provided by the 25 MV tandem accelerator at the Holifield Radioactive Ion Beam Facility (HRIBF) at Oak Ridge National Laboratory (ORNL).

The experimental setup included a HPGe Clover array, CLARION [36], a 2π CsI array, BareBall [37], and a Bragg-curve detector; the experimental setup was identical to that in Ref. [38], which provides further detail. By measuring the absolute cross sections and particle-γ angular correlations of excited states following Coulomb excitation on two separate targets, a complete set of electromagnetic moments were determined; cf. Refs. [10,17,32]. The absolute cross sections were obtained by measuring the Coulomb excitation to Rutherford scattering yield, i.e., the ratio of particle-γ and particle rates. The energy loss of the tin beams through the targets was directly measured with a zero-degree Bragg detector. The energy loss through the 1.01 mg/cm^2 carbon target was measured with a ^{114}Sn beam and was determined to be 78.4(17) and 78.0(17) MeV for beam energies of 2.53A and 2.9A MeV, respectively. The energy loss of the ^{114}Sn beam at 2.9A MeV through the 1.09 mg/cm^2 titanium target was 58.9(16) MeV.

The γ-ray spectra of $^{112-124}$Sn from Coulomb excitation on natural carbon and titanium targets are shown in Figs. 1(a)–1(g). The spectra are dominated by single-step excitation of the 2_1^+ state. There are several advantages to performing Coulomb excitation in inverse kinematics with a low-Z-carbon target, particularly for measuring absolute $B(E2; 0_1^+ \rightarrow 2_1^+)$ values, which include (1) the nucleus of interest is a pure beam and the composition of natural carbon (and other natural targets) is well known, (2) the excitation process is predominately single step, (3) the reorientation effect is minimized, (4) the target does not contribute to the γ-ray background, (5) the uncertainties are not limited by a target $B(E2)$ uncertainty (typical of relative measurements), and (6) the recoiling target nuclei are measured at backward center-of-mass angles where the Rutherford cross section is less sensitive to angle.

The extracted electromagnetic moments are given in Table I. Virtual excitations to higher-lying states and weak population of the 3_1^- state were included in the analysis using the Coulomb-excitation code GOSIA [39]; these effects were negligible for the carbon-target data. Because the $\langle 2_1^+ || M(E2) || 2_1^+ \rangle$ values only varied on average by 0.03 eb between positive and negative quadrupole interference signs, the average was adopted. Details of the analysis procedures, including necessary corrections, can be found in Refs. [10,17,32,38,40].

The g factors were determined by the recoil-in-vacuum (RIV) method, following the same analysis procedures as described recently for ^{124,126,128}Sn [17] and ^{134}Te [32]. The

TABLE I. Summary of first 2^+ electromagnetic moments.

$Z = 50$	N	$\langle 0_1^+ \|\| M(E2) \|\| 2_1^+ \rangle$ eb	$\langle 2_1^+ \|\| M(E2) \|\| 2_1^+ \rangle$ eb	$\|g\|\tau$ ps	$B(E2; 0_1^+ \rightarrow 2_1^+)$ e^{2}b^2	$Q(2_1^+)$ eb	g[a]
^{112}Sn	62	(+) 0.500(10)	+0.05(12)	0.078(22)	0.250(10)	+0.04(9)	+0.150(43)
^{114}Sn	64	(+) 0.479(10)	+0.12(11)	0.066(30)	0.229(9)	+0.09(8)	+0.138(63)
^{116}Sn	66	(+) 0.453(9)	+0.22(11)	0.000(35)	0.205(8)	+0.17(8)	0.000(64)
^{118}Sn	68	(+) 0.451(10)	+0.09(12)	0.000(55)	0.203(9)	+0.07(9)	0.000(77)
^{120}Sn[b]	70	(+) 0.458(10)		0.087(26)	0.210(9)		−0.099(30)
^{122}Sn	72	(+) 0.445(10)	−0.11(12)	0.000(51)	0.198(9)	−0.08(9)	0.000(48)
^{124}Sn	74	(+) 0.406(8)	−0.11(12)	0.129(14)	0.165(7)	−0.08(9)	−0.097(11)

[a] g-factor signs taken from transient field measurements [14–16,41] and τ derived from the $B(E2)$ values.
[b] Due to beam-time constraints, ^{120}Sn on titanium was omitted.

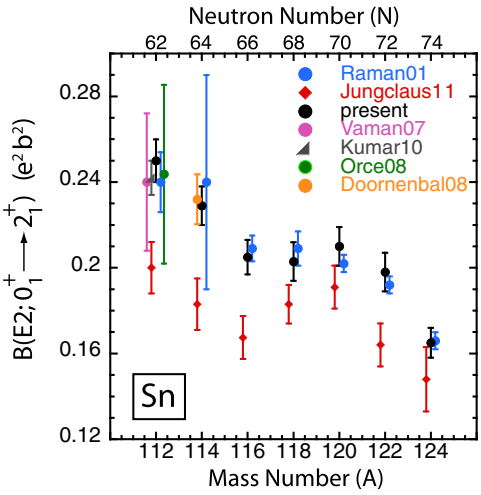

FIG. 2. (Color online) The stable tin $B(E2;0_1^+ \rightarrow 2_1^+)$ e^2b^2 systematics. The experimental data are taken from the present study and from Refs. [3,5,7–9,34].

product $|g|\tau$, where $|g|$ is the magnitude of the g factor and τ is the mean life, was determined from fits to the angular correlations for both the C and Ti targets. Signs of the g factors were taken from transient-field measurements [14–16,41], with which the present results are in overall agreement. The present result for ^{124}Sn is in excellent agreement with the previous RIV measurement [17]. It is noteworthy that $\tau(2_1^+) \sim 0.5$ ps in ^{112,114,116}Sn. These cases represent the shortest level lifetimes to date for which the RIV method has been applied. Our measurements establish that the RIV method can be applied to future g-factor measurements on the proton-rich isotopes towards ^{100}Sn for which the level lifetimes increase.

The stable tin $B(E2;0_1^+ \rightarrow 2_1^+)$ values from the present study, measured to a precision of ∼4%, are compared with the recent Doppler-shift attenuation results [9] and Raman evaluation [34] in Fig. 2. The magnitudes of the present $B(E2)$ values are consistent with the Raman evaluation, but the values for ^{112,114}Sn have been measured to higher precision, revealing a clear increase in collectivity below midshell. However, similar to the results of Jungclaus *et al.*, there is weak evidence for a local minimum near midshell within statistical uncertainty ($\sigma_{\text{statistical}} \leqslant 0.002\,e^2b^2$ or $\sigma_{\text{statistical}} \leqslant 0.9\%$, which is less than or equal to the size of the data points). Other recent measurements on ^{112}Sn by Vaman *et al.* [3] and Orce *et al.* [5] have uncertainties that are too large to distinguish between the discrepant values. Doornenbal *et al.* [7] and Kumar *et al.* [8] recently measured ^{114}Sn and ^{112}Sn, respectively, but their measurements were relative to ^{116}Sn; these relative measurements are unable to distinguish between the magnitude of the Jungclaus [9] and Raman [34] values.

The stable tin $Q(2_1^+)$ values from the present study are consistent with previous measurements from the 1970s [42–44]. However, the present results have been measured to much higher precision ($\sigma_{\text{total}} \sim 0.09$ eb and $\sigma_{\text{statistical}} \sim 0.02$ eb), include the effect of virtual excitations, include a value for ^{114}Sn, and reveal a bell-shaped trend with a maximum at midshell. The trend of the $Q(2_1^+)$ values appears to be

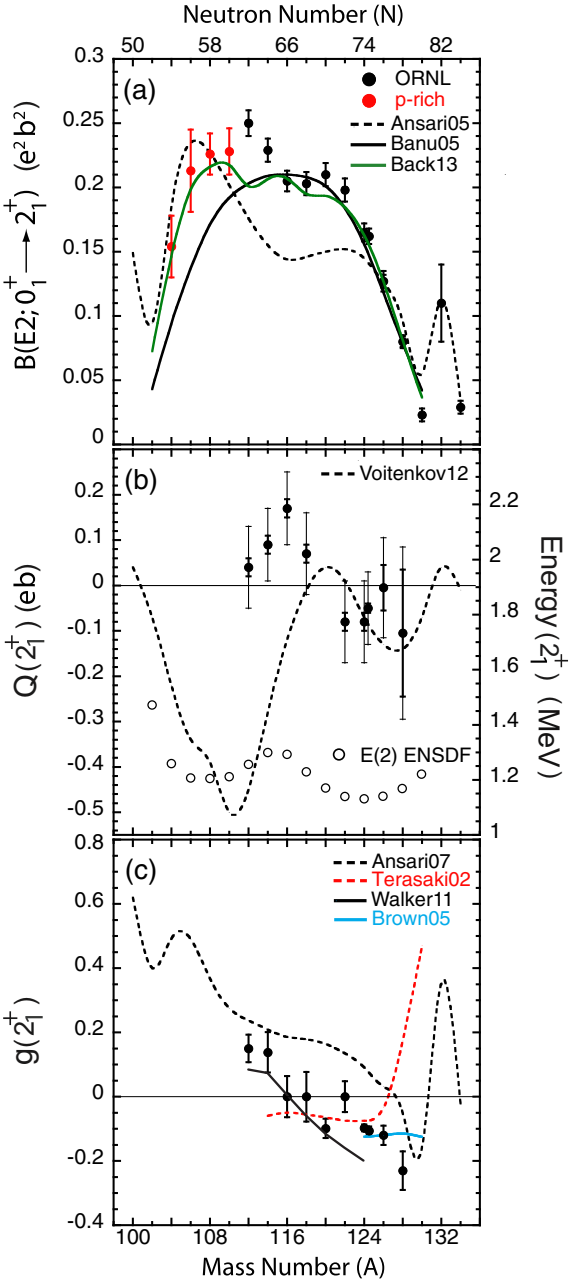

FIG. 3. (Color online) The first 2^+ electromagnetic-moment and energy systematics of the semimagic tin isotopes. The stable and neutron-rich data (black circles) are taken from the present and previous ORNL studies [1,10,17]. The proton-rich data (red circles) are taken from the linear-weighted average of Refs. [2–4,6,11–13]. The energies (open circles) are taken from the Evaluated Nuclear Structure Data File [45]. The theoretical curves are taken from QRPA-based (dashed lines) [20,21,25,46] and shell-model-based (solid lines) [2,15,19,27] calculations.

correlated with the trend of the 2_1^+ energies; cf. the γ-ray energies in Fig. 1.

A summary of the electromagnetic moments of the semimagic tin isotopes is given Fig. 3. The striking feature is that all three electromagnetic observables show a change in behavior near midshell. While all of the theory calculations

are able to reproduce some features of the experimental data, no single theory reproduces all of the data.

The $B(E2)$ calculations by Banu *et al.* [2], cf. Fig. 3(a), show excellent agreement above midshell but fail for $N \leqslant 64$. The large-scale shell-model (LSSM) calculations by Banu *et al.* were performed with a ^{100}Sn core, which represents the most simple expectation. Calculations with a ^{90}Zr core were also attempted to increase the magnitude of the $B(E2)$ values but the symmetric trend remained. Recent LSSM calculations by Back *et al.* [27] tried a different approach by including an isospin-dependent effective charge, which broke the $B(E2)$ symmetry about midshell. The use of an isospin-dependent effective charge greatly improves the overall agreement with experiment but it fails to describe the sudden rise in collectivity for ^{112,114}Sn. The relativistic quasiparticle random-phase approximation (RQRPA) calculations by Ansari [20] show some qualitative agreement with the general shape of the experimental $B(E2)$ values but the calculations fail to reproduce the magnitude of the midshell region. The experimental $B(E2)$ values show an overall enhancement compared with the recent theoretical calculations. None of the calculations are able to accurately describe the $B(E2)$ values of ^{112}Sn and ^{114}Sn.

The recent QRPA-based calculations of $Q(2_1^+)$ by Voitenkov *et al.* [25], cf. Fig. 3(b), are consistent with the experimental data for the heavier isotopes but show serious inconsistencies for ^{112,114,116}Sn. While the uncertainties of the experimental $Q(2_1^+)$ values are on the order of $\sim$0.09 eb, the statistical uncertainties are only $\sim$0.02 eb, which are shown in Fig. 3(b) by the inner error bars. Within statistical uncertainty, the experimental $Q(2_1^+)$ values show a clear maximum at midshell, ^{116}Sn; this maximum is not quantitatively or qualitatively described by the calculations of Voitenkov *et al.* [25].

The general trend in the g factors reflects the single-particle orbits at the Fermi surface. The positive g factors for ^{112,114}Sn are associated with occupation of the $g_{7/2}$ orbit, whereas for ^{124}Sn and the heavier isotopes toward ^{132}Sn, the occupation of the $h_{11/2}$ orbit results in a negative $g(2^+)$. The recent LSSM calculations of $g(2_1^+)$ by Walker *et al.* [15], cf. Fig. 3(c), are in fairly good agreement with the experimental data. The same is true for the LSSM calculations by Brown *et al.* [19]. The RQRPA calculations by Ansari and Ring [21] agree with the general shape of the experimental $g(2_1^+)$ values but not the magnitude, similar to the situation with the $B(E2)$ values. The QRPA calculations by Terasaki *et al.* [46] are consistent with the data up to ^{126}Sn but show a dramatic increase afterwards. Unfortunately, the sign of the g factor of ^{128}Sn has not been measured but is inferred from systematics [17].

None of the recent LSSM or QRPA calculations appear capable of reproducing all of the features of the 2_1^+ electromagnetic moments. Invoking core excitations and isospin-dependent effective charges [2,27] alone do not resolve the $B(E2)$ discrepancies between theory and experiment. There is likely a rich mixture of physics occurring that will require many simultaneous ingredients such as (a) core excitations to increase the overall $B(E2)$ magnitudes [2], (b) isospin-dependent effective charges to break the $B(E2)$ symmetry [27], (c) $s_{1/2}$ suppression of collectivity near midshell [9,23], and (d) possible $N = 64$ subshell effects. Furthermore, the newly discovered trend in the $Q(2_1^+)$ values, which shows a maximum at midshell, ^{116}Sn, appears to be correlated with the trend of the 2_1^+ energies, cf. Fig. 3(b). It is also interesting to note that the 2p-2h and 4p-4h intruders, which are outside of the current model spaces, are lowest in energy at midshell (see Ref. [47] and references therein). These deformed intruder states are known to mix with the ground and first-excited 2_1^+ states [48]; this mixing could be partly responsible for the $Q(2_1^+)$ and $B(E2)$ trends near midshell. The role of the 2p-2h and 4p-4h intruders on the 2_1^+ energies and electromagnetic moments needs to be investigated experimentally and theoretically in the future. Multistep Coulomb excitation of ^{116}Sn to measure the $E2$ matrix elements of the intruder bands, e.g., $Q(2^+_{\text{intruder}})$, would be a good place to start.

Another interesting perspective emerges from a recent proton inelastic scattering study of ^{104}Sn and ^{112}Sn by Corsi *et al.* [18]; to our knowledge this is the only published (p,p′) study of an unstable tin isotope. The inelastic (p,p′) cross sections are sensitive to both the neutron and proton transition matrix elements, M_n and M_p, where $M_p(L) = \sqrt{B(EL)/(2L+1)}$. Corsi *et al.* reported a 40(24)% drop in the 2_1^+ inelastic-scattering cross section from ^{112}Sn to ^{104}Sn versus a 26(12)% drop in the $B(E2)$ value; using the $B(E2)$ values from the present study results in a 38(10)% drop. These results indicate that the proton and neutron collectivities are proportional within uncertainty over a relatively large range in neutron number. Because the neutron field strength is a factor of $\sim$2.25 larger than the proton field strength [18] for a beam energy of $\sim 130A$ MeV, these results also indicate that the collectivity of the 2_1^+ state is dominated by the neutrons, i.e., $M_n > M_p$, which is the simple expectation for a closed proton shell. Corsi *et al.* conclude from their QRPA calculations that the asymmetry in the experimental $B(E2)$ values about midshell is likely induced by an enhancement in the neutron collectivity. A continuation of (p,p′) studies to other tin isotopes, particularly with higher precision, would be of significant value for quantifying the proton and neutron contributions to the 2_1^+ wave function and elucidating the origin of the $B(E2)$ asymmetry. High-precision $B(E2)$ values, such as those in the present study, will be required in extracting M_n values from future (p,p′) studies. Moreover, the nature of the observed increase in collectivity below midshell would benefit from g-factor measurements, like those presented here, which are sensitive to the proton versus neutron contributions to the wave function.

In conclusion, a complete set of electromagnetic moments, $B(E2; 0_1^+ \rightarrow 2_1^+)$, $Q(2_1^+)$, and $g(2_1^+)$, have been measured from Coulomb excitation of semimagic ^{112,114,116,118,120,122,124}Sn ($Z = 50$) on natural carbon and titanium targets. The magnitudes of the $B(E2)$ values disagree with a recent lifetime study by Jungclaus *et al.* [9] that employed the Doppler-shift attenuation method; the discrepancies are of similar magnitude to some of the differences between recent theoretical calculations. The $B(E2)$ values show an overall enhancement compared with recent theoretical calculations and a clear asymmetry about midshell. All of the recent calculations fail to describe the $B(E2)$ values of ^{112,114}Sn. A new static electric quadrupole moment, $Q(2_1^+)$, has been measured for ^{114}Sn. The static quadrupole moments reveal a bell-shaped trend with a maximum at midshell,

^{116}Sn, which is not described by recent theory. The trend of the $Q(2_1^+)$ values appears to be correlated with the trend of the 2_1^+ energies. The magnetic dipole moments exhibit a near-monotonic decrease in value with neutron number, going through a change of sign near midshell. Current-theory calculations fail to reproduce the electromagnetic moments of the tin isotopes. The role of 2p-2h and 4p-4h intruders, which are lowest in energy at midshell and outside of current model spaces, may be responsible for some of the observed trends in the electromagnetic moments near midshell and their role needs to be investigated in the future. Furthermore, the proton and neutron contributions to the 2_1^+ wave function need further investigation from additional (p,p′) studies with higher precision, and also g-factor measurements, which have been shown to be feasible with the RIV method for the tin isotopes towards ^{100}Sn. The stable and exotic tin isotopes have been and will continue to be a prototypical benchmark of state-of-the-art theory and experiment.

ACKNOWLEDGMENTS

The authors gratefully acknowledge D. Cline, A.B. Hayes, N. Warr, and J.L. Wood for fruitful discussions, J.P. Greene (Argonne National Laboratory) for making the carbon and titanium targets, and the HRIBF operations staff for providing the beams used in this study. This material is based upon work supported by the U.S. Department of Energy, Office of Science, Office of Nuclear Physics and this research used resources of the Holifield Radioactive Ion Beam Facility of Oak Ridge National Laboratory, which is a DOE Office of Science User Facility. This research was also sponsored by the Australian Research Council under Grant No. DP0773273, by CONACyT (Mexico) under Grant No. CB103366, and by the National Science Foundation. In addition, this work was supported in part by the U.S. DOE under Contracts No. DE-AC05-76OR00033 (UNIRIB), No. DE-FG02-96ER40963 (UTK), and No. DE-FG52-08NA28552 (Rutgers).

[1] D. C. Radford *et al.*, Nucl. Phys. A **752**, 264c (2005).
[2] A. Banu *et al.*, Phys. Rev. C **72**, 061305(R) (2005).
[3] C. Vaman *et al.*, Phys. Rev. Lett. **99**, 162501 (2007).
[4] J. Cederkäll *et al.*, Phys. Rev. Lett. **98**, 172501 (2007).
[5] J. N. Orce *et al.*, Phys. Rev. C **76**, 021302(R) (2007); **77**, 029902(E) (2008).
[6] A. Ekström *et al.*, Phys. Rev. Lett. **101**, 012502 (2008).
[7] P. Doornenbal *et al.*, Phys. Rev. C **78**, 031303(R) (2008).
[8] R. Kumar *et al.*, Phys. Rev. C **81**, 024306 (2010).
[9] A. Jungclaus *et al.*, Phys. Lett. B **695**, 110 (2011).
[10] J. M. Allmond *et al.*, Phys. Rev. C **84**, 061303(R) (2011).
[11] G. Guastalla *et al.*, Phys. Rev. Lett. **110**, 172501 (2013).
[12] V. M. Bader *et al.*, Phys. Rev. C **88**, 051301(R) (2013).
[13] P. Doornenbal *et al.*, Phys. Rev. C **90**, 061302(R) (2014).
[14] M. C. East, A. E. Stuchbery, A. N. Wilson, P. M. Davidson, T. Kibédi, and A. I. Levon, Phys. Lett. B **665**, 147 (2008).
[15] J. Walker *et al.*, Phys. Rev. C **84**, 014319 (2011).
[16] G. J. Kumbartzki *et al.*, Phys. Rev. C **86**, 034319 (2012).
[17] J. M. Allmond *et al.*, Phys. Rev. C **87**, 054325 (2013).
[18] A. Corsi *et al.*, Phys. Lett. B **743**, 451 (2015).
[19] B. A. Brown, N. J. Stone, J. R. Stone, I. S. Towner, and M. Hjorth-Jensen, Phys. Rev. C **71**, 044317 (2005).
[20] A. Ansari, Phys. Lett. B **623**, 37 (2005).
[21] A. Ansari and P. Ring, Phys. Lett. B **649**, 128 (2007).
[22] L. Y. Jia, H. Zhang, and Y. M. Zhao, Phys. Rev. C **75**, 034307 (2007).
[23] I. O. Morales, P. Van Isacker, and I. Talmi, Phys. Lett. B **703**, 606 (2011).
[24] N. Lo Iudice, Ch. Stoyanov, and D. Tarpanov, Phys. Rev. C **84**, 044314 (2011).
[25] D. Voitenkov, S. Kamerdzhiev, S. Krewald, E. E. Saperstein, and S. V. Tolokonnikov, Phys. Rev. C **85**, 054319 (2012).
[26] H. Jiang, Y. Lei, G. J. Fu, Y. M. Zhao, and A. Arima, Phys. Rev. C **86**, 054304 (2012).
[27] T. Bäck, C. Qi, B. Cederwall, R. Liotta, F. Ghazi Moradi, A. Johnson, R. Wyss, and R. Wadsworth, Phys. Rev. C **87**, 031306(R) (2013).
[28] H. Jiang, Y. Lei, C. Qi, R. Liotta, R. Wyss, and Y. M. Zhao, Phys. Rev. C **89**, 014320 (2014).
[29] L. Coraggio, A. Covello, A. Gargano, N. Itaco, and T. T. S. Kuo, Phys. Rev. C **91**, 041301(R) (2015).
[30] K. L. Jones *et al.*, Nature (London) **465**, 454 (2010).
[31] J. Van Schelt *et al.*, Phys. Rev. Lett. **111**, 061102 (2013).
[32] A. E. Stuchbery *et al.*, Phys. Rev. C **88**, 051304(R) (2013).
[33] J. M. Allmond *et al.*, Phys. Rev. Lett. **112**, 172701 (2014).
[34] S. Raman, C. W. Nestor, and P. Tikkanen, At. Data Nucl. Data Tables **78**, 1 (2001).
[35] D. C. Radford *et al.*, Phys. Rev. Lett. **88**, 222501 (2002).
[36] C. J. Gross *et al.*, Nucl. Instrum. Methods Phys. Res., Sect. A **450**, 12 (2000).
[37] A. Galindo-Uribarri, AIP Conf. Proc. **1271**, 180 (2010).
[38] J. M. Allmond *et al.*, Phys. Rev. C **90**, 034309 (2014).
[39] T. Czosnyka *et al.*, Bull. Am. Phys. Soc. **28**, 745 (1983); www.pas.rochester.edu/∼cline/Gosia/.
[40] J. M. Allmond *et al.*, J. Phys.: Conf. Ser. **639**, 012007 (2015).
[41] M. Hass, C. Broude, Y. Niv, and A. Zemel, Phys. Rev. C **22**, 97 (1980).
[42] A. M. Kleinfeld *et al.*, Nucl. Phys. A **154**, 499 (1970).
[43] P. H. Stelson *et al.*, Phys. Rev. C **2**, 2015 (1970).
[44] R. Graetzer *et al.*, Phys. Rev. C **12**, 1462 (1975).
[45] Evaluated Nuclear Structure Data File (ENSDF), http://www.nndc.bnl.gov/ensdf/
[46] J. Terasaki, J. Engel, W. Nazarewicz, and M. Stoitsov, Phys. Rev. C **66**, 054313 (2002).
[47] K. Heyde and J. L. Wood, Rev. Mod. Phys. **83**, 1467 (2011).
[48] J. Kantele *et al.*, Z. Phys. A: At. Nucl. **289**, 157 (1979).